

Modulation of graphene field effect by heavy charged particle irradiation

Edward Cazalas, Biddut K. Sarker, Isaac Childres, Yong P. Chen, and Igor Jovanovic

Citation: *Appl. Phys. Lett.* **109**, 253501 (2016); doi: 10.1063/1.4972398

View online: <http://dx.doi.org/10.1063/1.4972398>

View Table of Contents: <http://aip.scitation.org/toc/apl/109/25>

Published by the [American Institute of Physics](#)

Articles you may be interested in

[Ultra-fine metal gate operated graphene optical intensity modulator](#)

Appl. Phys. Lett. **109**, 251101 (2016); 10.1063/1.4972306

[Nanoscale deformations in graphene by laser annealing](#)

Appl. Phys. Lett. **109**, 253102 (2016); 10.1063/1.4972845

[Investigation of electron irradiation-induced magnetism in layered MoS₂ single crystals](#)

Appl. Phys. Lett. **109**, 252403 (2016); 10.1063/1.4971192

[Valley splitting of single-electron Si MOS quantum dots](#)

Appl. Phys. Lett. **109**, 253101 (2016); 10.1063/1.4972514

Modulation of graphene field effect by heavy charged particle irradiation

Edward Cazalas,^{1,a)} Biddut K. Sarker,^{2,3,b)} Isaac Childres,^{2,3} Yong P. Chen,^{2,3,4} and Igor Jovanovic^{1,5}

¹Department of Mechanical and Nuclear Engineering, The Pennsylvania State University, University Park, Pennsylvania 16802, USA

²Department of Physics and Astronomy, Purdue University, West Lafayette, Indiana 47907, USA

³Birck Nanotechnology Center, Purdue University, West Lafayette, Indiana 47907, USA

⁴School of Electrical and Computer Engineering, Purdue University, West Lafayette, Indiana 47907, USA

⁵Department of Nuclear Engineering and Radiological Sciences, University of Michigan, Ann Arbor, Michigan 48109, USA

(Received 30 September 2016; accepted 3 December 2016; published online 19 December 2016)

Device architectures based on the two-dimensional material graphene can be used for sensing of electromagnetic and particle radiation. The sensing mechanism may be direct, by absorbance of radiation by the graphene or the immediately adjacent material, and indirect, via the field effect principle, whereby the change in conductivity within a semiconducting absorber substrate induces electric field change at graphene. Here, we report on a graphene field effect transistor (GFET) sensitive to heavy charged particle radiation (α particles) at MeV energies by use of the indirect sensing mechanism. Both the continuous and discrete changes of graphene are observed, and the latter are attributed to single α particle interactions with the GFET. While this study provides the basis for understanding of the irradiation effects, it also opens prospects for the use of GFETs as heavy charged particle detectors. *Published by AIP Publishing.* [<http://dx.doi.org/10.1063/1.4972398>]

Graphene's sensitivity to changes in the local electric field makes it a promising material for implementation in a variety of sensor architectures.^{1–3} It has been demonstrated that the unique properties of graphene can be used to develop graphene-based sensors to detect molecules, including those relevant for biochemical processes,^{4–9} low-energy electromagnetic radiation,^{10–16} and ionizing radiation, such as electrons, X rays, and gamma rays.^{17–22}

Graphene can be used as a direct or indirect sensor. Direct sensing relies on the direct interaction of radiation, atoms, or compounds with the graphene, for example, by absorption,^{23–28} or with a material immediately adjacent to graphene, such as a quantum dot or a nanomaterial layer deposited on graphene.^{29–33} In these architectures, graphene current is modulated by the excitation of electrons within graphene or in the nanomaterial immediately adjacent to graphene.^{34–36} In contrast, indirect sensing relies on the interaction of penetrating radiation with an underlying semiconducting substrate. In this approach, graphene is placed on a back-gated undoped semiconductor substrate in a graphene field effect transistor (GFET), as shown in Fig. 1(a). The energy deposited by the radiation modifies the conductivity of the substrate by production of electron-hole pairs, which are then transported within the substrate. The modification of substrate conductivity modulates the graphene current via the field effect principle, whereby the measured graphene current is sensitive to changes in the local electric field.^{37–39}

Graphene-based devices have been used to sense photons, molecules, and high fluxes of charged particles by

observing the graphene properties change due to its damage.^{17,40–44} However, the interaction of heavy charged particles with the GFET at relatively low particle fluxes (on the order of $10^3 \text{ cm}^{-2} \text{ s}^{-1}$ and lower) and high energies (on the order of MeV) has not been studied to date. Here, we investigate the effect of alpha (α) particle irradiation on the electrical response of a GFET. We first examine the graphene current response to α particle exposure at positive and negative gate polarities for two different radioactive sources. Next, we reveal the discrete step-like response of graphene, attributed to single α particle interaction, particularly for the negative gate polarity. Finally, we employ a simple electronic device model and Monte Carlo simulation to support the conclusions made from experimental measurements.

In a GFET, α particles are detected by measuring the change of the graphene current, I_{sd} , which occurs when the conductivity of the substrate is modified by ionization from α particle depositions in the substrate. The GFET studied in this work consists of graphene on a back-gated substrate. The dimensions of graphene are $20 \times 4 \mu\text{m}^2$ (see [supplementary material](#) Section I for additional information on GFET fabrication). The change of substrate conductivity acts to modify the electric field that is present in the vicinity of graphene, as illustrated in Figs. 1(b) and 1(c), before and after a single α particle absorption, respectively. For a change in graphene current to be attributed to α particles and be distinguishable from noise, the magnitude of the field effect must be sufficiently large. The magnitude of the field effect is dependent on the rate of α particle absorption in the substrate, the location of α particle absorption relative to the graphene, and the energy of the α particles.

Time-dependent, $I_{sd} - t$, and voltage-dependent, $I_{sd} - V_g$, measurements were conducted, which are used to evaluate

^{a)}Author to whom correspondence should be addressed. Electronic mail: edward.cazalas@gmail.com. Now at Air Force Institute of Technology, 2950 Hobson Way, Wright-Patterson AFB, OH 45433, USA.

^{b)}Now at INFICON Inc., 2 Technology Pl., East Syracuse, New York 13057, USA.

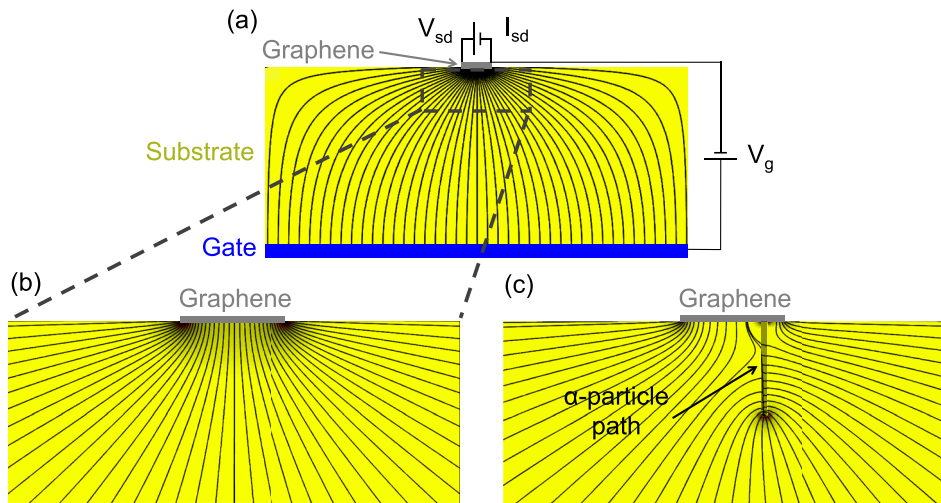


FIG. 1. (a) Back-gated GFET on the undoped SiC substrate. Application of gate voltage creates an electric field within the substrate. (b) Enlargement section of Fig. 1(a) showing the shape of the electric field under graphene. (c) A 3-MeV α particle deposits energy and modifies conductivity along its path. Conductivity change increases electric field strength at graphene, inducing the field effect.

the GFET response to α particle absorption and survey the field effect characteristics of the GFET. Measurement results with exposure to a ^{210}Po source and ^{241}Am source are shown in Fig. 2(a). These field effect measurements were taken after stabilization of the field effect or continuous exposure to ^{241}Am and ^{210}Po sources at $V_g = -60\text{ V}$ for 5 min and 3 h, respectively. A greater field effect was observed when the higher activity (^{241}Am) α source was used. This is expected due to the greater change of substrate conductivity as the rate of ionization in the substrate is increased. As shown in Fig. 2(b), the difference in field effect characteristics for non-exposure and exposure to the ^{210}Po source at $V_g = -40\text{ V}$ is measurable; the magnitude of this difference is important in interpretation of single α absorption events. The gate voltage at which all the field effect curves intercept is expected to be $V_g = 0\text{ V}$. Due to a possible combination of the effect of built-up charge in the substrate and doping of graphene by the ambient environment and during fabrication, the intercept gate voltage is shifted to positive V_g , whereby an additional application of electric field is required to induce an effective zero doping in graphene.^{45–48}

Time-dependent measurements of graphene current resulted in a greater rate of change of I_{sd} when GFET was exposed to the higher activity ^{241}Am source compared to the lower activity ^{210}Po source, as shown in Figs. 3(a) and 3(b). Also, as predicted from the field effect characteristic measurements, $I_{sd} - V_g$, a greater rate of change of graphene current is observed for negative gate voltages. The total

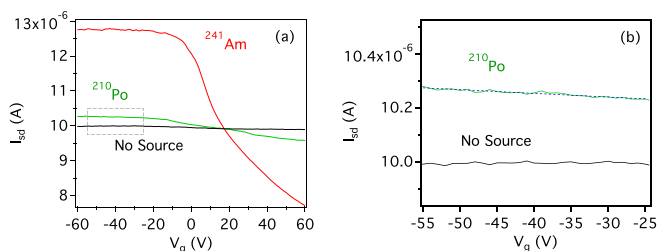


FIG. 2. (a) Graphene field effect when unexposed and exposed to ^{241}Am and ^{210}Po α particle sources is shown. (b) An enlarged view from the dotted box in (a) shows a negligible field effect with GFET unexposed and field effect due to ^{210}Po α source exposure. A blue dotted line provides a linear fit to the $I_{sd} - V_g$ measurement with ^{210}Po exposure in the range of $-55\text{ V} < V_g < -25\text{ V}$.

exposure times of the GFET were 35 min and 11 h for the ^{241}Am and the ^{210}Po source, respectively.

As shown in Fig. 3(b), during measurements at $V_g = -40\text{ V}$ with the ^{210}Po source exposure, I_{sd} exhibits discrete increasing steps. These discrete steps are shown in detail in supplementary material Section V. When the time derivative of the time-dependent current is calculated, the relatively fast and large step changes in I_{sd} are made more apparent and appear as spikes, as in Fig. 3(d). The discrete steps in I_{sd} are attributed to individual α particles depositing their energy directly under or near the edge of the graphene, which is corroborated by the following analysis: first, the electric field in the sensitive region of the substrate near graphene is modeled; second, energy deposition spectra of α particles expected in this sensitive region are calculated. The slow recovery of graphene current after α particle exposure is likely due to doping of graphene.

The electric field in the GFET was modeled using the COMSOL Multiphysics framework.⁴⁹ A region of modified conductivity was defined corresponding to energy deposition by a 3-MeV α particle, which is a typical energy deposited in the substrate by α particles from the ^{210}Po source, accounting

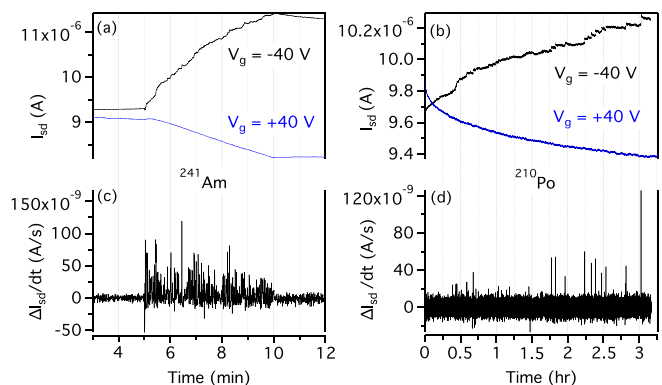


FIG. 3. $I_{sd} - t$ measurements for exposure over (a) 5 min ($t = 5\text{--}10\text{ min}$) to the ^{241}Am α source and (b) 3 h (for $t > 10\text{ min}$) to the ^{210}Po α source. (c) Time derivative of $I_{sd} - t$ measurements, with GFET exposed to ^{241}Am α source for $V_g = -40\text{ V}$ shows positive spikes, indicating positive changes in I_{sd} , attributed to α particle energy deposition into the substrate. (d) For time derivative of $I_{sd} - t$ measurements with ^{210}Po α source exposure for $V_g = -40\text{ V}$, discrete positive spikes are attributed to single α particle energy depositions into the substrate under or near graphene.

for energy loss in air in our experiment and the source energy spectrum (a range of 1.88 cm is calculated for a 5 MeV α particle slowing to 3 MeV in air). Additional information about the model and related calculations is provided in [supplementary material Section III](#). As shown in Fig. 1(c), when the modified conductivity region is present, the electric field lines are partially diverted toward the region where the α particle deposits its energy and where the conductivity is increased, and then toward graphene. To quantify the effect of this reconfiguration of the electric field near graphene, the average electric field along the width of graphene is plotted as a function of the distance (x) of the modified conductivity region from the center under graphene, $x = 0 \mu\text{m}$ (Fig. 4(c)).

The electric field at graphene maintains an increased magnitude when energy deposition occurs under graphene but drops rapidly at the edge of graphene ($x = 2 \mu\text{m}$ in Fig. 4(c)). The electric field reaches the magnitude equal to that when no modified conductivity region is present at a relatively small distance from the center of graphene, $x \approx 3 \mu\text{m}$. These characteristic distances obtained from the two-dimensional model and shown in Fig. 4(c) correspond to the width of graphene in our GFET ($2 \mu\text{m}$); the model was also applied to the orthogonal dimension (graphene length, $20 \mu\text{m}$), obtaining the result that the electric field is increased up to several μm from outside the edge of graphene. Thus, the area over which the GFET is sensitive to ionization extends over the region $-3 \leq x \leq 3 \mu\text{m}$ (along graphene width) and $-15 \leq y \leq 15 \mu\text{m}$ (along graphene length), or approximately as far as half of the graphene width or length beyond the edge of graphene. We define the highly sensitive region as $-2.1 < y < 2.1 \mu\text{m}$ (along graphene width) and $-10.25 < x < 10.25 \mu\text{m}$ (along graphene length) corresponding to a sensitive area of $20.5 \times 4.2 \mu\text{m}^2$. This represents an area within which the electric field is modified by $>50\%$ of the difference between the electric field at the center of graphene ($x = 0 \mu\text{m}$) and the electric field at $x = 3 \mu\text{m}$, corresponding to no modification of the electric field due to α exposure.

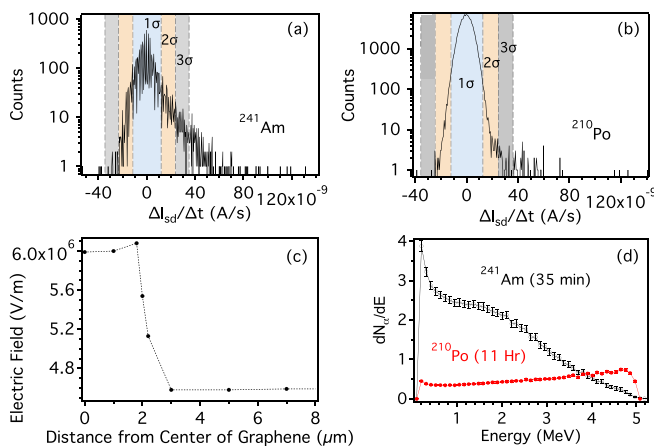


FIG. 4. Distribution of the time derivative of the $I_{sd} - t$ measurement with GFET exposure to (a) the ^{241}Am α source (total experimental time, $t_e = 35$ min) and (b) the ^{210}Po α source ($t_e = 11$ h). (c) The plot shows modification to electric field by 3-MeV α particle energy deposition for one half of the graphene (graphene center at $0 \mu\text{m}$ and the edge at $2 \mu\text{m}$). (d) Simulated energy deposition spectra in the effective area of graphene for time, t_e , with exposure to ^{241}Am (unfilled circles) and ^{210}Po (filled circles) α sources.

The occurrence of single α particle sensing can be further supported by the analysis of the discrete step changes in I_{sd} (Figs. 3(b) and 3(d)), the field effect measurements (Fig. 2(b)), and the electric field model (Fig. 4(c)). The change of the electric field due to a single discrete absorption event in experiment can be determined from the change in graphene current and compared to the modeled change in electric field due to single α particle absorption. The change in electric field due to α particle absorption in Fig. 4(c) is $\approx 1.4 \times 10^6$ V/m or $\approx 24\%$. At $V_g = -40$ V, a 24% change of electric field would correspond to a change of back-gate voltage of approximately -10 V. The effect of this change of back-gate voltage on the current through graphene (I_{sd}) can then be estimated from the independently measured $I_{sd} - V_g$ characteristic when graphene is exposed to the ^{210}Po source (Fig. 2(b)). A linear fit, $I_{sd} = a + bV_g$, with fit parameters of $a = 1.02 \times 10^5$ A and $b = -1.367 \times 10^9$ A V $^{-1}$, is obtained from the $I_{sd} - V_g$ measurement in the range -55 V $< V_g < -25$ V. Typical large discrete steps of I_{sd} in Fig. 3(b) can be estimated as $\approx 1.5 \times 10^{-8}$ A. Using the linear fit, a discrete step change of $I_{sd} = 1.5 \times 10^{-8}$ A corresponds to a back-gate voltage change $\Delta V_g \approx -11$ V, which is of the order of the change in V_g predicted from the correlation of the electric field model (Fig. 4(c)) and $I_{sd} - V_g$ measurement (Fig. 2(b)). This analysis further establishes the correspondence between the electric field model to experimental $I_{sd} - t$ and $I_{sd} - V_g$ measurements and supports the conclusion that individual α particle interactions with the GFET are observed.

A Monte Carlo simulation was conducted to calculate the energy deposition spectra of α particles depositing energy under the effective area of graphene ($20.5 \times 4.2 \mu\text{m}^2$). Additional information on the Monte Carlo simulation is provided in [supplementary material Section IV](#). The resulting energy deposition spectra for the region under the effective area of graphene for the α sources are shown in Fig. 4(d), and the information on the number of simulated α particles depositing energy under the effective area of graphene is given in Table I (α_{t_e} [sim]). The number of α particles counted in the experiment is obtained from the distribution of the time derivative of the time-dependent graphene current ($I_{sd} - t$), shown in Figs. 4(a) and 4(b). The simulation provides an estimate of the rate of α particle incidence onto the effective area of GFET, which can be compared to the rate of discrete steps appearing in $I_{sd} - t$ measurements. A good agreement is observed between the predicted (simulated) and experimentally measured rate of discrete steps

TABLE I. The number of α particles detected in experiment compared with simulation. α_{t_e} [sim] is the simulated number of α particles absorbed in the substrate for measurement period t_e ; α_{t_e} [exp] is the number of α particles detected within the bins shown in Figs. 4(a) and 4(b) at $V_g = -40$ V during t_e . $t_e = 35$ min and $t_e = 11$ h for GFET exposure to the ^{241}Am and ^{210}Po α sources, respectively. The value of α_{t_e} [exp] is calculated by summing all events (as in Fig. 4(a) or 4(b)) above a given standard deviation (noise).

	α_{t_e} [sim]	α_{t_e} [exp]			
		σ	2σ	3σ	4σ
^{241}Am	72.1 ± 3.7	960	355	162	67
^{210}Po	22.9 ± 1.24	526	72	45	21

appearing in the $I_{sd} - t$ measurement for the ^{210}Po source at $V_g = -40\text{ V}$. The standard deviations are shown in the histograms of Figs. 4(a) and 4(b). The agreement further supports the hypothesis that the observed discrete steps in $I_{sd} - t$ when the GFET is exposed to the ^{210}Po source are due to individual α particles depositing energy within the effective area of the GFET.

While the discrete steps in $I_{sd} - t$ are discernible when the ^{210}Po source is used, as in Figs. 3(b) and 3(d), this is not the case when the GFET is exposed to the ^{241}Am source, as in Fig. 3(a) or 3(c). This is attributed to the difference between the energy spectra of the ^{210}Po and ^{241}Am sources. As shown by simulation (Fig. 4(d)), the absorbed energy spectrum from the ^{241}Am source is weighted to lower energies, while the spectrum for the ^{210}Po source is weighted to higher energies. Thus, when the GFET is irradiated by the ^{210}Po source, a greater fraction of α particles incident on the GFET have the high energies needed to produce a large, discrete response. In contrast, the greater fraction of lower energy α particles emitted by the ^{241}Am source may obscure any discrete steps that occur in $I_{sd} - t$ measurements. The higher incidence rate of α particles from the ^{241}Am source induces a relatively large continuous rate of change in I_{sd} ; however, since the majority of α particles have lower energy, each particle causes only a small change of the substrate conductivity. Large numbers of such small energy depositions incrementally and collectively act to produce a significant change of conductivity. Conversely, the much lower rate of α particle absorption by the substrate when exposed to the ^{210}Po source allows for identification of discrete steps, especially as the average energy deposited by an α particle from the ^{210}Po source is higher. Discrete steps in $I_{sd} - t$ measurements are not discernible for either source when positive gate voltage is applied ($V_g = +40\text{ V}$), as in Fig. 3(b). This is believed to be due to the lower field effect response of the GFET for positive gate voltage ($V_g = 40\text{ V}$) compared to negative gate voltage ($V_g = -40\text{ V}$), as also observed in field effect measurements in Fig. 2, especially for the ^{241}Am source. The greater sensitivity at negative gate voltage is believed to be due to the greater difference between the measurement voltage at $V_g = -40\text{ V}$ and the charge neutrality point at approximately $V_g = +20\text{ V}$ (as shown in Fig. 2(a)). Finally, measurements of a “dummy” device exposed to the ^{241}Am source, where graphene is replaced with gold, show no response to α particle exposure, as discussed in [supplementary material](#) Section VI.

In conclusion, experiments were conducted to develop an understanding of the effect of heavy charged particle irradiation on GFET electrical response. The GFETs consist of CVD graphene on SiC substrates in a back-gated architecture. The graphene field effect and time dependent response to α particle exposure from ^{241}Am and ^{210}Po radioisotope sources for both positive and negative gate voltages have been studied. For both α particle sources, a greater field effect is measured for negative gate voltages (V_g), which is likely due to doping of the graphene. Time-dependent measurements show cumulative graphene current response to both ^{241}Am and ^{210}Po sources, with greater current response for the higher activity ^{241}Am source. These time-dependent measurements are consistent with field effect measurements.

Of particular interest are the discrete step-like changes in graphene current when exposed to the ^{210}Po source at negative gate voltage. These discrete changes of graphene current are attributed to absorption of individual α particles in the area directly under graphene or near the edge of graphene. An analysis was conducted that includes an electric field model and Monte Carlo simulation. The results of the analysis support the single α particle sensitivity hypothesis by predicting the magnitude of change of the electric field at graphene due to single α particle absorption under graphene comparable to that observed in the experiment. The analysis also shows that the predicted number of α particles in simulation is in agreement with the number of discrete changes in graphene current for the ^{210}Po source.

Future work should focus on detailed experimental quantification of the dependence of discrete graphene current changes on the energy depositions of single charged particles in a GFET. To accurately perform such experiments, a monoenergetic particle source with ability to control both the particle energy and particle flux is desirable.

The experiments and analyses conducted within this work advance the understanding of charged particle interaction with GFETs and represent a step toward the utilization of graphene-based devices as ionizing radiation sensors operating in the pulse (single event) mode. GFETs could provide benefits of scalability to large sizes while maintaining low-power operation. In addition to the established sensing of electromagnetic radiation, GFETs show promise as heavy charged particle detectors for a variety of scientific and engineering applications.

See [supplementary material](#) for more detail on the GFET fabrication process, calculation of conductivity within the substrate, experimental setup, and electrical measurements. Also discussed are the Monte Carlo simulation method, testing of dummy devices, and the effects of radiation damage on graphene.

This work was funded by the Department of Homeland Security (DHS) and the National Science Foundation (NSF) through the Academic Research Initiative (ARI) (2009-DN-077-ARI036-02) and by the Defense Threat Reduction Agency (DTRA).

- ¹A. K. Geim and K. S. Novoselov, *Nat. Mater.* **6**, 183 (2007).
- ²A. H. Castro Neto, F. Guinea, N. M. R. Peres, K. S. Novoselov, and A. K. Geim, *Rev. Mod. Phys.* **81**, 109 (2009).
- ³K. S. Novoselov, V. I. Fal'ko, L. Colombo, P. R. Gellert, M. G. Schwab, and K. Kim, *Nature* **490**, 192 (2012).
- ⁴F. Schedin, A. K. Geim, S. V. Morozov, E. W. Hill, P. Blake, M. I. Katsnelson, and K. S. Novoselov, *Nat. Mater.* **6**, 652 (2007).
- ⁵P. K. Ang, W. Chen, A. T. S. Wee, and K. P. Loh, *J. Am. Chem. Soc.* **130**, 14392 (2008).
- ⁶Y. Shao, J. Wang, H. Wu, J. Liu, I. Aksay, and Y. Lin, *Electroanalysis* **22**, 1027 (2010).
- ⁷M. Pumera, *Mater. Today* **14**, 308 (2011).
- ⁸Y. Liu, X. Dong, and P. Chen, *Chem. Soc. Rev.* **41**, 2283 (2012).
- ⁹F. Yan, M. Zhang, and J. Li, *Adv. Healthcare Mater.* **3**, 313 (2014).
- ¹⁰F. Xia and P. Avouris, *IEEE Photonics J.* **3**, 293 (2011).
- ¹¹L. Vicarelli, M. S. Vitiello, D. Coquillat, A. Lombardo, A. C. Ferrari, W. Knap, M. Polini, V. Pellegrini, and A. Tredicucci, *Nat. Mater.* **11**, 865 (2012).
- ¹²M. Mittendorff, S. Winnerl, J. Kamann, J. Eroms, D. Weiss, H. Schneider, and M. Helm, *Appl. Phys. Lett.* **103**, 021113 (2013).

- ¹³C.-h. Liu, Y.-c. Chang, T. B. Norris, and Z. Zhong, *Nat. Nanotechnol.* **9**, 273 (2014).
- ¹⁴C. G. Kang, S. K. Lee, T. J. Yoo, W. Park, U. Jung, J. Ahn, and H. B. Lee, *Appl. Phys. Lett.* **104**, 161902 (2014).
- ¹⁵F. H. L. Koppens, T. Mueller, P. Avouris, A. C. Ferrari, M. S. Vitiello, and M. Polini, *Nat. Nanotechnol.* **9**, 780 (2014).
- ¹⁶B. Sarker, E. Cazalas, I. Childres, I. Jovanovic, and Y. Chen, in *APS Meeting Abstracts* (2015), Vol. 1, p. 17003.
- ¹⁷I. Childres, L. A. Jauregui, M. Foxe, J. Tian, R. Jalilian, I. Jovanovic, and Y. P. Chen, *Appl. Phys. Lett.* **97**, 173109 (2010).
- ¹⁸A. Patil, O. Koybasi, G. Lopez, M. Foxe, I. Childres, C. Roecker, J. Boguski, J. Gu, M. L. Bolen, M. A. Capano, I. Jovanovic, P. Ye, and Y. P. Chen, in *IEEE Nuclear Science Symposium and Medical Imaging Conference (NSS/MIC)* (2011), pp. 455–459.
- ¹⁹C. D. Cress, J. G. Champlain, I. S. Esqueda, J. T. Robinson, A. L. Friedman, and J. J. McMorrow, *IEEE Trans. Nucl. Sci.* **59**, 3045 (2012).
- ²⁰I. S. Esqueda, C. D. Cress, T. J. Anderson, J. R. Ahlbin, M. Bajura, M. Fritze, and J.-S. Moon, *Electronics* **2**, 234 (2013).
- ²¹O. Koybasi, E. Cazalas, I. Childres, I. Jovanovic, and Y. P. Chen, in *IEEE Nuclear Science Symposium and Medical Imaging Conference (NSS/MIC)* (2013), pp. 1–6.
- ²²E. Cazalas, B. K. Sarker, M. E. Moore, I. Childres, Y. P. Chen, and I. Jovanovic, *Appl. Phys. Lett.* **106**, 223503 (2015).
- ²³F. Xia, T. Mueller, Y.-m. Lin, A. Valdes-garcia, and P. Avouris, *Nat. Nanotechnol.* **4**, 839 (2009).
- ²⁴N. M. Gabor, J. C. W. Song, Q. Ma, N. L. Nair, T. Taychatanapat, K. Watanabe, T. Taniguchi, L. S. Levitov, and P. Jarillo-Herrero, *Science* **334**, 648 (2011).
- ²⁵B. Chitara, L. S. Panchakarla, S. B. Krupanidhi, and C. N. R. Rao, *Adv. Mater.* **23**, 5419 (2011).
- ²⁶M. Freitag, T. Low, and P. Avouris, *Nano Lett.* **13**, 1644 (2013).
- ²⁷B. Y. Zhang, T. Liu, B. Meng, X. Li, G. Liang, X. Hu, and Q. J. Wang, *Nat. Commun.* **4**, 1811 (2013).
- ²⁸X. Cai, A. B. Sushkov, R. J. Suess, M. M. Jadidi, G. S. Jenkins, L. O. Nyakiti, R. L. Myers-Ward, S. Li, J. Yan, D. K. Gaskill, T. E. Murphy, H. D. Drew, and M. S. Fuhrer, *Nat. Nanotechnol.* **9**, 814 (2014).
- ²⁹Y. Lin, K. Zhang, W. Chen, Y. Liu, Z. Geng, J. Zeng, N. Pan, L. Yan, X. Wang, and J. G. Hou, *ACS Nano* **4**, 3033 (2010).
- ³⁰Y. Liu, R. Cheng, L. Liao, H. Zhou, J. Bai, G. Liu, L. Liu, Y. Huang, and X. Duan, *Nat. Commun.* **2**, 579 (2011).
- ³¹G. Konstantatos, M. Badioli, L. Gaudreau, J. Osmond, M. Bernechea, F. P. G. de Arquer, F. Gatti, and F. H. L. Koppens, *Nat. Nanotechnol.* **7**, 363 (2012).
- ³²P. Afzali, Y. Abdi, and E. Arzi, *J. Nanopart. Res.* **16**, 2659 (2014).
- ³³Y.-J. Lin and S.-H. Yang, *Appl. Phys. A* **116**, 91 (2014).
- ³⁴D. Sun, G. Aivazian, A. M. Jones, J. S. Ross, W. Yao, D. Cobden, and X. Xu, *Nat. Nanotechnol.* **7**, 114 (2012).
- ³⁵M. Freitag, T. Low, F. Xia, and P. Avouris, *Nat. Photonics* **7**, 53 (2013).
- ³⁶Y. Xu, Z. Li, and W. Duan, *Small* **10**, 2182 (2014).
- ³⁷T. J. Echtermeyer, M. C. Lemme, J. Bolten, M. Baus, M. Ramsteiner, and H. Kurz, *Eur. Phys. J. - Spec. Top.* **148**, 19 (2007).
- ³⁸B. K. Sharma and J.-H. Ahn, *Solid-State Electron.* **89**, 177 (2013).
- ³⁹B. Zhan, C. Li, J. Yang, G. Jenkins, W. Huang, and X. Dong, *Small* **10**, 4042 (2014).
- ⁴⁰L. Tapasztó, G. Dobrik, P. Nemes-Incze, G. Vertesy, P. Lambin, and L. P. Biró, *Phys. Rev. B* **78**, 233407 (2008).
- ⁴¹G. Compagnini, F. Giannazzo, S. Sonde, V. Raineri, and E. Rimini, *Carbon* **47**, 3201 (2009).
- ⁴²M. Lucchese, F. Stavale, E. M. Ferreira, C. Vilani, M. Moutinho, R. B. Capaz, C. Achete, and A. Jorio, *Carbon* **48**, 1592 (2010).
- ⁴³O. Ochedowski, B. Kleine Bussmann, B. Ban d'Etat, H. Lebius, and M. Schleberger, *Appl. Phys. Lett.* **102**, 153103 (2013).
- ⁴⁴O. Ochedowski, K. Marinov, G. Wilbs, G. Keller, N. Scheuschner, D. Severin, M. Bender, J. Maultzsch, F. J. Tegude, and M. Schleberger, *J. Appl. Phys.* **113**, 214306 (2013).
- ⁴⁵H. Wang, Y. Wu, C. Cong, J. Shang, and T. Yu, *ACS Nano* **4**, 7221 (2010).
- ⁴⁶P. L. Levesque, S. S. Sabri, C. M. Aguirre, J. Guillemette, M. Sjaaj, P. Desjardins, T. Szkopek, and R. Martel, *Nano Lett.* **11**, 132 (2011).
- ⁴⁷H. Xu, Y. Chen, J. Zhang, and H. Zhang, *Small* **8**, 2833 (2012).
- ⁴⁸E. Cazalas, I. Childres, A. Majcher, T.-F. Chung, Y. P. Chen, and I. Jovanovic, *Appl. Phys. Lett.* **103**, 053123 (2013).
- ⁴⁹COMSOL Multiphysics®, 2014. Version 5 COMSOL, Inc., Burlington, MA, USA.